Probabilistic Northern Hemisphere Freeze/Thaw Data Record derived from Satellite Multi-Frequency Microwave Brightness Temperatures

Version 1.0 Release

Contact Information:
Jinyang Du and John S. Kimball
Numerical Terradynamic Simulation Group (NTSG)
The University of Montana
Missoula MT, 59812
Email: johnk@ntsg.umt.edu; jinyang.du@umontana.edu.

Project URL: http://freezethaw.ntsg.umt.edu

Release date: 2023-12-15

Acknowledgements: This work was conducted at the University of Montana under contract to NASA. The associated data record was generated under the NASA MEaSUREs (Making Earth System Data Records for Use in Research Environments) and ABoVE (Arctic Boreal Vulnerability Experiment) programs (80NSSC18K0980, 80NSSC22K1238).

Contents:

1 - INTRODUCTION

This document provides information relating to a probabilistic Northern Hemisphere freeze/thaw (FT) data record derived using a deep learning model (U-Net) architecture informed by satellite multi-frequency microwave brightness temperature retrievals from the NASA SMAP (Soil Moisture Active Passive) and JAXA AMSR2 (Advanced Microwave Scanning Radiometer 2) radiometers, and trained using daily soil temperature observations from Northern Hemisphere weather stations and global reanalysis data (ERA-5). Unlike other available FT data records that provide only a binary (0,1) classification of frozen or non-frozen conditions, this product includes both binary FT and continuous variable estimates of the probability of thawed conditions. This product is designed to complement other established binary FT data records, including the NASA FT Earth System Data Record (Kim et al. 2021) and SMAP Level 3 FT operational products (Xu et al. 2020), by providing a probabilistic FT variable with enhanced accuracy and sensitivity to near-surface (≤5 cm depth) soil FT conditions.

The biophysical importance of the FT retrieval from satellite microwave remote sensing is well established, providing an effective proxy of the timing, extent and duration of frozen conditions in the landscape (McDonald and Kimball 2006). Over half (~66 million km^2) of the global land area experiences seasonal FT processes profoundly affecting surface meteorology and hydrologic activity, vegetation productivity and ecological trace gas dynamics (Kim et al. 2017, Parazoo et al. 2018). Microwave sensors are uniquely capable of detecting and monitoring FT status owing to their strong sensitivity to changes in the relative abundance of liquid water as the landscape transitions between

predominantly frozen and thawed states. The lower frequency (~ ≤ K_u-band) measurements available from many operational polar-orbiting satellites are also insensitive to solar illumination and atmospheric contamination, enabling consistent, near-daily observations day-or-night and under nearly all-weather conditions. However, different microwave frequencies have varying sampling footprints and FT sensitivities to different landscape features, including vegetation, snow, and soil conditions. Low frequency (L-band) measurements have greater characteristic soil sensitivity (Entekhabi et al. 2010), while the addition of complimentary higher frequency measurements can further enhance soil FT detection by increasing the information content of the retrievals and reducing potential noise contributed from other landscape features (Bateni et al. 2013, Du et al. 2017).

A detailed description of the underlying methods and product validation is provided elsewhere (Donahue et al. 2023), while a summary of the soil FT data record and product format is provided below. Unlike other satellite microwave FT environmental data records that commonly provide a bulk landscape level FT retrieval, this product quantifies soil FT conditions in the near-surface (0-5cm depth) soil layer. The resulting data product has favorable accuracy and consistent performance suitable for scientific research, and the soil FT parameter is expected to have greater utility in defining frozen soil constraints on soil moisture availability, permafrost stability, soil organic matter decomposition and soil respiration processes contributing to greenhouse gas emissions. Future product releases may include refinements to the data format and an extended data record enabled from ongoing SMAP and AMSR operations.

2 - Data Description

This daily data record includes both binary and probabilistic FT variables produced using the same deep learning framework and geospatial inputs. The model inputs include: rSIR spatially enhanced vertically and horizontally polarized brightness temperatures (T_Bs) from SMAP (1.4 GHz) (Brodzik et al. 2022) and overlapping AMSR2 (18.7 and 36.5 GHz) T_B retrievals (Maeda et al. 2016) mapped to a consistent Northern Hemisphere polar grid. The T_B retrievals include both ascending (6am SMAP; 1:30pm AMSR2) and descending (6am SMAP; 1:30am AMSR2) local orbital overpass sampling times. Additional model inputs include the DEM derived mean elevation and latitude of each 9-km resolution grid cell. The product contains daily local morning (6am) and evening (6pm) FT predictions spanning the data years from 2016 through 2020. The beginning of the data record is defined by the first complete calendar year of SMAP observations. All model inputs and outputs are formatted to the Northern Hemisphere Polar EASE-Grid 2 projection (Brodzik et al. 2014) consistent with the Polar Enhanced Resolution (PER) FT-ESDR (Kim et al. 2021). The 9-km product grid resolution is also

consistent with the resolution of the rSIR T_B inputs and the SMAP enhanced L3 radiometer Northern Hemisphere FT product (Xu et al. 2020).

This product is intended to provide a reliable soil FT classification for all non-permanently frozen lands in the Northern Hemisphere, along with enhanced spatial information, accuracy, and soil FT sensitivity gained from the use of complimentary multi-frequency T_B inputs. The combined use of SMAP L-band (1.4 GHz) T_B observations and AMSR2 higher frequency T_B retrievals as key inputs to a U-Net deep learning model, trained using soil FT observations from both model data reanalysis and in situ soil temperature network measurements, provides enhanced product sensitivity to FT conditions in the near-surface soil layer (Donahue et al. 2023). The resulting product includes a continuous variable estimate of the probability of thawed conditions, which may have enhanced information and utility for some applications (Farhadi et al. 2015, Zwieback et al. 2012).

An example of the product outputs showing the probability of frozen conditions for four selected days in 2016 is shown in **Figure 1**. The U-Net model outputs and associated product includes a daily binary FT classification (0 for frozen, 1 for thawed) for all land areas on a 9km polar grid, along with a continuous FT classification ranging from low (0) to high (1) probability of thawed conditions on the same grid. Masked grid cells (e.g. black areas in Fig. 1) include cells dominated by open water, permanent Ice cover, or permanently frozen land as defined by a land-ice-ocean mask (Friedl et al. 2010). The model is trained from independent soil temperature observations to recognize and classify FT transitions across a prescribed 0ºC thermal boundary between predominantly frozen and thawed ground conditions. Here, the model inputs are sensitive to the large characteristic T_B response to changes in near-surface liquid water abundance and associated dielectric properties that occur during landscape FT transitions. The combined use of different frequencies and polarizations provide additional information to better distinguish soil FT transitions from other landscape FT contributions from lower atmosphere, snow and vegetation components of the sensor footprint. The product includes different daily fields for local morning and afternoon FT conditions, which are derived from similarly trained but separate models using ascending and descending overpass T_B inputs.

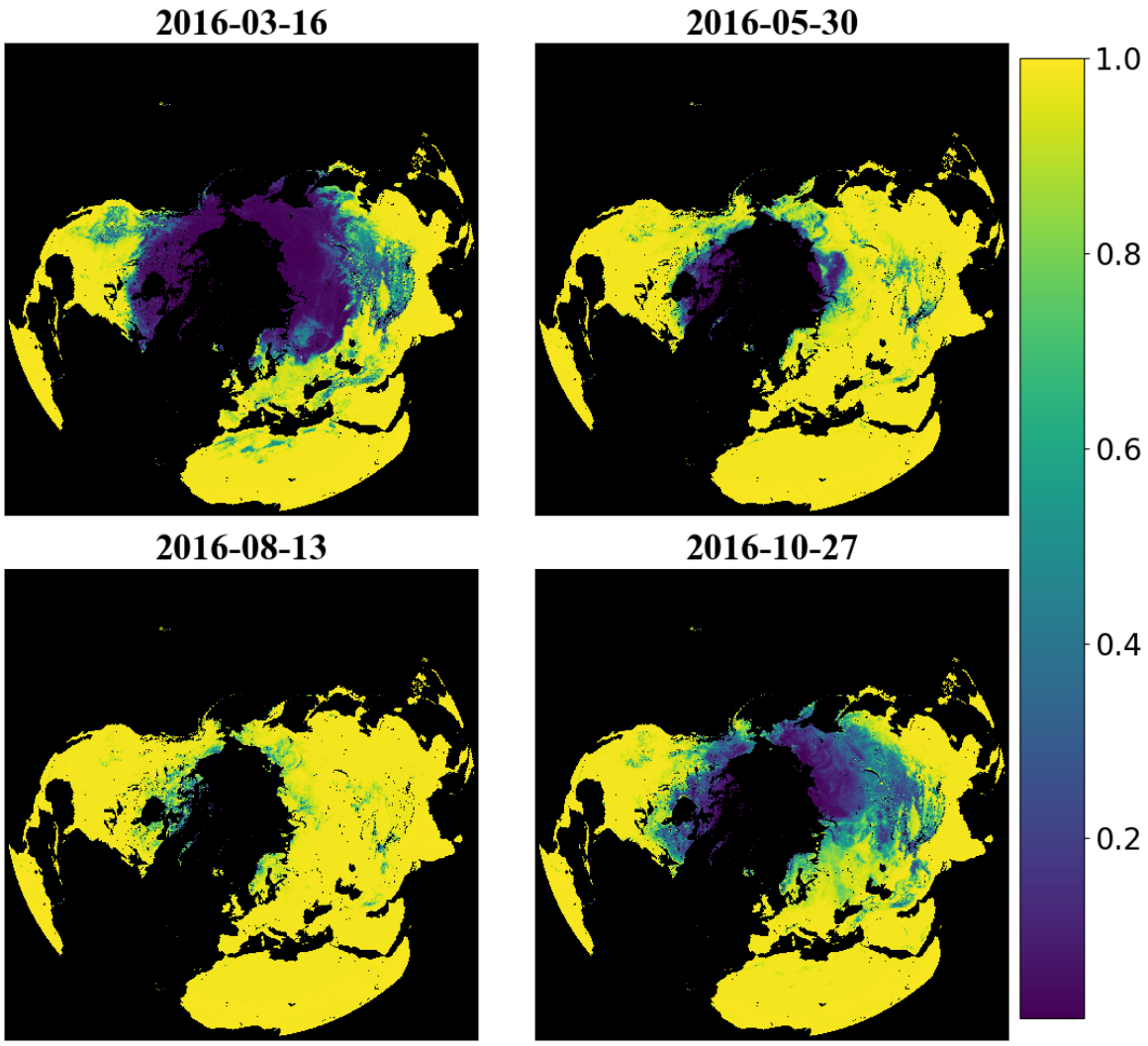

Figure 1*: Example product fields showing the probability of thawed conditions for four selected days over the 2016 seasonal cycle. The probability of thawed conditions ranges from low (0) to high (1) and is lower at higher latitudes and upper elevations during early spring (Mar) and late fall (Oct) in the Northern Hemisphere; in contrast, the probability of thawed conditions is much greater during mid-summer (Aug).*

3 - Accuracy and performance

The product was validated using a combination of in-situ soil (≤5cm depth) temperature measurements from Northern Hemisphere weather stations and ERA5 Reanalysis surface layer (Layer 1) soil temperature data. The in-situ soil temperature measurements were used for the primary validation, but were supplemented with ERA5 temperatures to compensate for the sparse weather station network (***Figure 3***). The daily temperature records were converted to FT prior to the validation assessment using

a 0ºC threshold to distinguish between frozen and non-frozen conditions. The morning and afternoon FT product fields were then compared against the respective 6am and 6pm readings of the temperature observations. These times were selected to represent diurnal conditions more likely to be uniform in soil temperature and soil dielectric properties, while also matching the SMAP orbital overpass times.

A summary of the product accuracy for a selected data year (2016) is shown in **Table 1**. The overall product accuracy for the morning (6am) FT data is 93.1% when compared to ERA5 and 92.5% compared to the in situ soil temperature measurements. The relative accuracy varies seasonally, ranging from 98.7% in the summer months to 89.6% in the winter months. The product also shows variable performance in different regions, as shown relative to ERA5 (***Figure 2***) and in-situ weather station (***Figure 3***) soil temperature records. The relative product accuracy is generally lower over complex mountain terrain such as the Rocky Mountains and Himalayas due to the scale mismatch between the coarse satellite T_B measurement footprint relative to the larger FT heterogeneity driven by the complex topography. The product accuracy is also lower over the Tibetan Plateau, where the complex terrain and arid landscape may reduce the effective microwave FT signal. Despite the above limitations, the product performance is similar or better than the accuracy reported from other available FT products from SMAP and the ESDR baseline (Kim et al. 2017, Derksen et al. 2017, Kim et al. 2019).

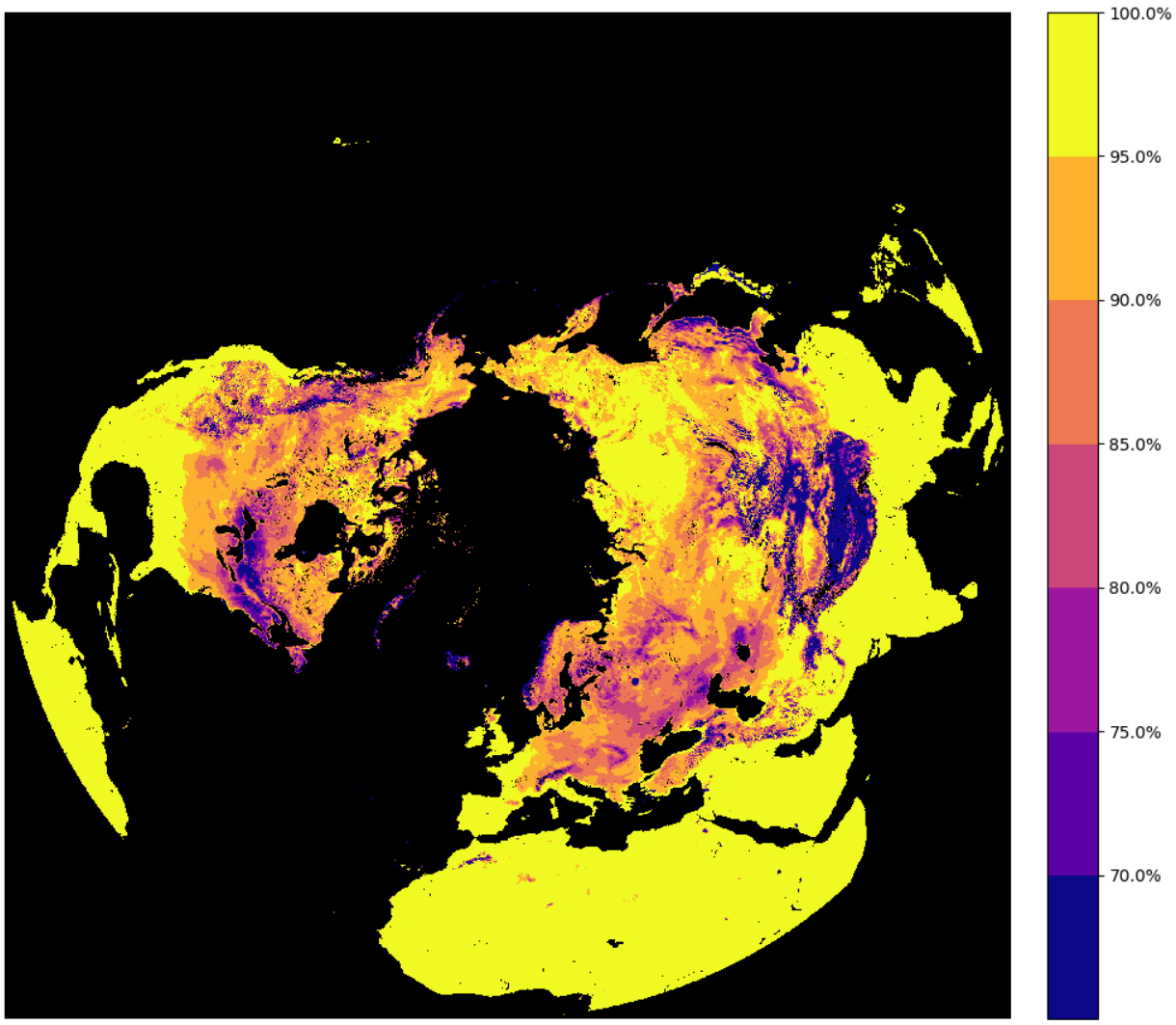

Figure 2: *Mean percent accuracy of the product in relation to ERA5 temperature based FT data for selected data year 2016. Black areas denote masked regions outside of the product domain.*

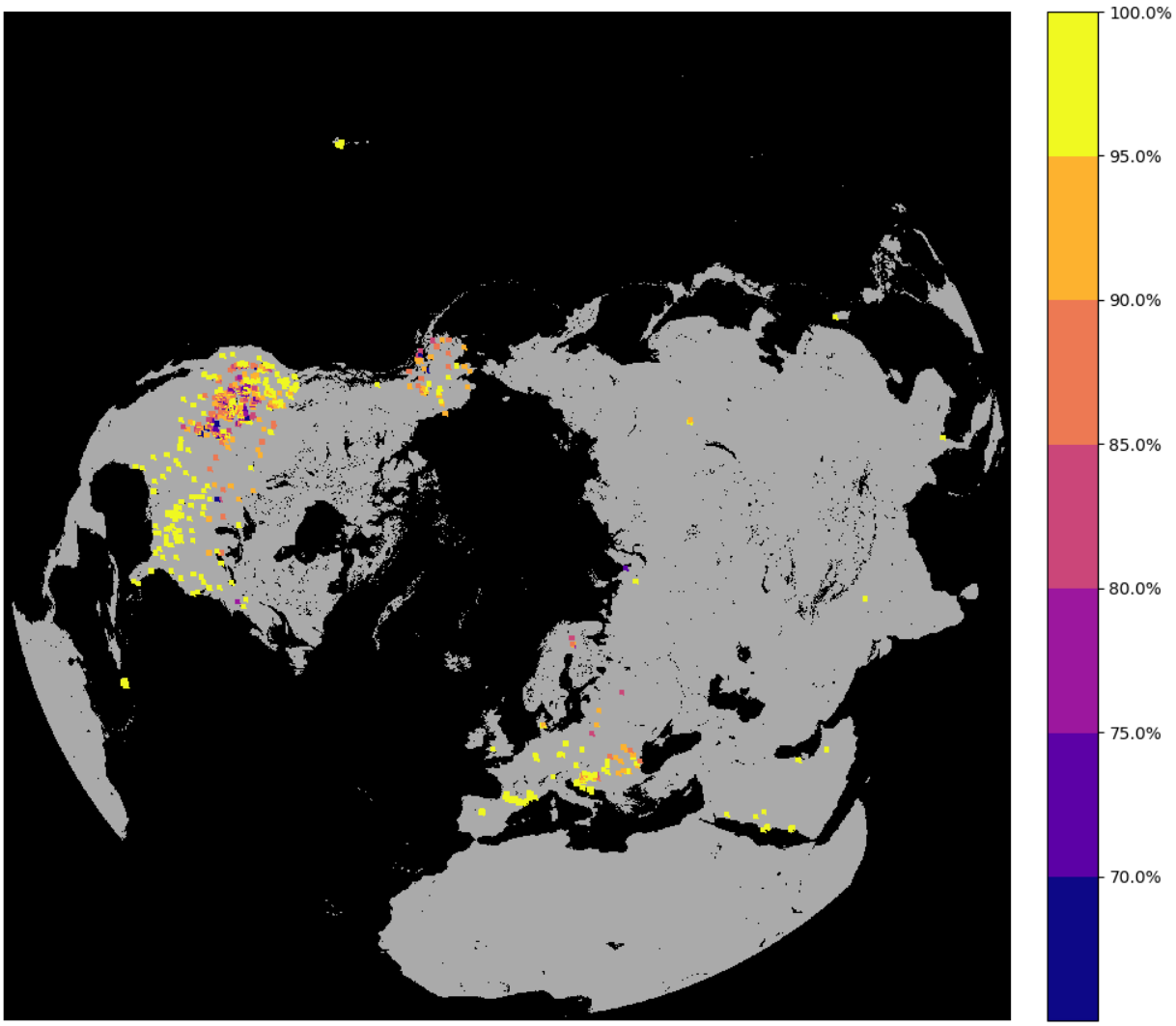

Figure 3: *Mean percent accuracy of the product in relation to soil temperature measurement based FT data from the regional weather station network for selected data year 2016. Approximately 700 stations were used in the validation assessment. Black areas denote masked regions outside of the product domain.*

4 - Ancillary Data used for Model Inputs and Training

The SMAP T_B record used to derive the FT product was obtained from the SMAP rSIR enhanced grid product (Brodzik et al. 2021), which is provided in a 9km polar EASE-grid 2 projection consistent with the FT product format and with spatially enhanced gridding and favorable performance relative to the SMAP native (~40-km) T_B sampling footprint (Long et al. 2023). Land recordings occur at approximately two-day intervals for land areas poleward of 45ºN, with consistent 6pm/am local ascending/descending orbital

overpass sampling times for the vertical and horizontal polarization T_B retrievals. The SMAP rSIR period of record used for processing begins March 31, 2015 and extended to May 1, 2021 at the time of this study. To construct complete daily records for each morning and afternoon T_B time series, missing T_B data between satellite swathes were gap-filled using a weighted average between the two most recent adjacent retrievals within up to a five-day moving window, as:

$$T_{missing} = T_{prev} * (1 - \frac{D_{prev}}{D_{prev}+D_{next}}) + T_{next} * (1 - \frac{D_{next}}{D_{prev}+D_{next}}) \quad (1)$$

In the above equation, $T_{missing}$ is the missing data being filled at a given location and time step, T_{prev} is the most recent valid data before a missing data value in the time series; T_{next} is the most recent data after the missing data value, D_{prev} is the number of days between $T_{missing}$ and T_{prev}, and D_{next} is the number of days between $T_{missing}$ and T_{next}. If no T_B data is present in the five-day window then the pixel is masked out to prevent gaps from being filled with data too temporally distant.

The AMSR2 T_B data was obtained for the 18.7 GHz and 36.5 GHz channels and vertical and horizontal polarizations overlapping with the same period of record as SMAP. The AMSR2 data were obtained in a consistent 10 km resolution global EASE-grid format from the AMSR2 GCOM-W Level3 product available through the JAXA G-Portal. The AMSR2 T_B retrievals include twice-daily coverage at higher latitudes owing to a relatively wide sensor swath and consistent 1:30am/pm local sampling from the orbital swath retrievals. Missing data was gap-filled in the same manner as the SMAP data (above). The AMSR2 data was then reprojected to the 9km polar EASE-grid 2 format using the LinearNDInterpolator from the scipy package. A linear interpolation method was chosen to provide a smooth reprojection of the data that considers all nearby cells when calculating the values for the grid. Other ancillary and temporally static model inputs included the latitude of each grid cell and a global digital elevation model (Danielson and Gesch 2011) aggregated from the 1-km native resolution to the 9-km polar EASE-grid 2.0 projection. A global land cover map (Friedl et al. 2010) was used to identify and mask grid cells dominated by large water bodies, permanent ice and snow, and other non-soil areas from the model domain.

In-situ daily soil temperature measurements from ~800 northern hemisphere weather stations were used for model training. The soil temperature records were obtained from available Northern Hemisphere stations, including Water and Climate Information System (USDA NRCS 2017), International Soil Moisture Network (Dorigo et al. 2021), Global Terrestrial Network for Permafrost (GTN-P), and GLOBE networks. The distribution of stations for the selected year 2016 is shown in **Figure 4**. For each station

location, we only used the shallowest soil temperature readings (within 5 cm depth) with local measurements obtained as close as possible to the 6am and 6pm SMAP sampling times. The location of each station measurement was assigned to the nearest grid cell in the 9km polar EASE-grid. If multiple stations were assigned to the same grid cell then the associated temperatures were averaged to produce the bulk value of the cell at each time step. The morning and afternoon temperature measurements were then classified into FT categories using a 0ºC FT threshold.

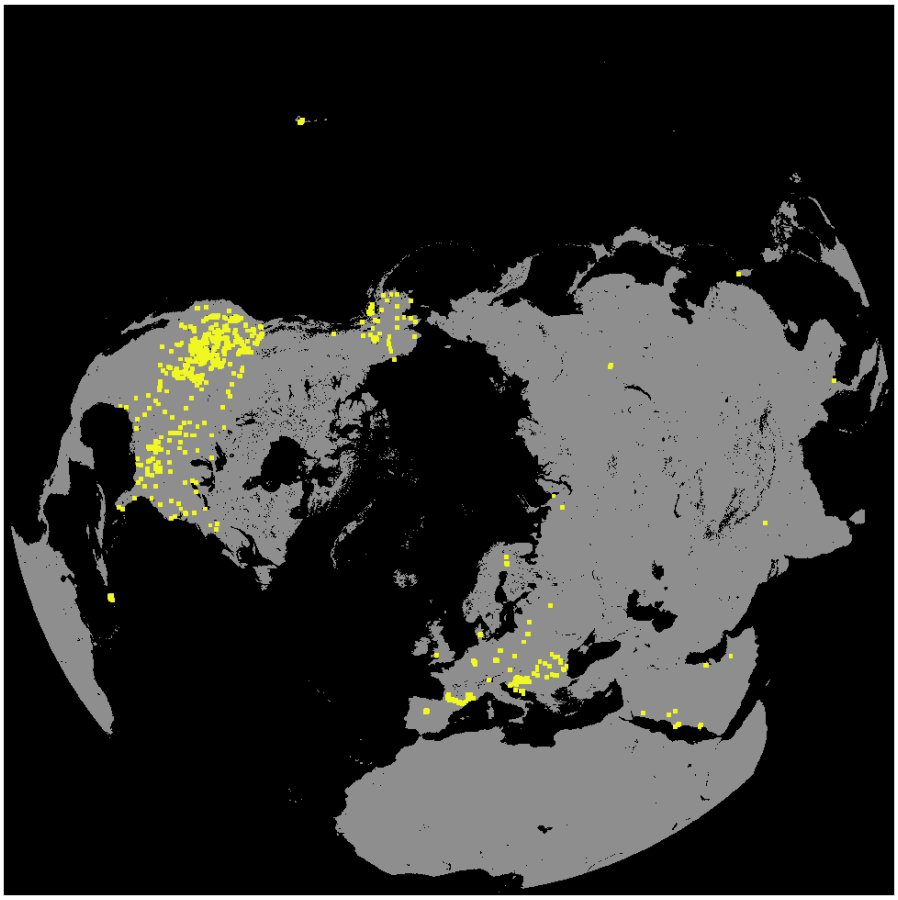

Figure 4: *Map of weather station locations with in situ soil temperature measurements for the year 2016. Approximately 800 stations were used in the analysis.*

The station temperature measurements reflect actual ground conditions useful for model validation, but the stations lack consistent sampling and are sparsely located. The actual number of station measurements also varies over time or may not be representative of the coarser model and satellite footprints, which can introduce uncertainty. To compensate for the limitations of the sparse station measurement network we also included daily surface layer temperatures from ECMWF ERA5 global

reanalysis data. ERA5 is a state-of-the-art model and data reanalysis product produced in a global 30 km resolution and hourly time step (Hersbach et al. 2020). For this study we used the ERA5 daily 6am and 6pm surface temperature (Layer 1) readings. The ERA5 temperature data was reprojected to the 9 km polar EASE-grid 2 projection using the same method as the AMSR2 data. ERA5 temperatures were also converted to FT values using the same procedure as was used for the in situ temperature processing. Because ERA5 is still a model output instead of a direct measurement, we put more weight on the station temperature measurements for the model training and validation, although the station measurements also have limitations as noted above.

5 – U-Net Architecture

The deep learning model U-Net architecture used to derive the soil FT product employs convolutional neural network learning with 4 downscaling and 4 upscaling layers and an initial filter bank size of 32 channels (**Figure 5**). The U-Net architecture is effective for satellite image segmentation (Ulmas and Liiv 2020, McGlinchy et al. 2019) including delineating FT patterns from satellite multi-frequency microwave brightness temperatures (Donahue et al. 2023). U-Net works by first running the geospatial inputs through multiple steps of convolutional blocks followed by max pool downsampling operations. The model dynamic inputs include multi-band (1.4, 18.7, 36.5 GHz) V and H polarized brightness temperature daily image arrays from SMAP and AMSR2. The U-Net downsampling convolutions condense the amount of spatial information while enhancing feature information. The process is then reversed with transposed convolution upsampling operations followed by convolutional blocks to take the condensed feature information and use it to construct the high resolution segmented output in the form of FT patterns. After each upsampling process, the corresponding downsampling information is concatenated through a skip connection to reintroduce the original spatial information to the data. Each convolutional block contains two sequences of a 3x3 convolution followed by a 2d batch normalization and a leaky ReLU activation function. The primary difference in our model to the standard U-Net is the inclusion of spatial dropout layers at the end of each convolutional block with a dropout rate of 20%. Dropout is used alongside a strong L2 weight normalization of 1e-3 to prevent over saturation of model weights. This is a particular concern due to the sparse station temperature data used for model training, which could lead to overfitting in pixels with station observations and cause areas of differing predictions to surrounding grid cells.

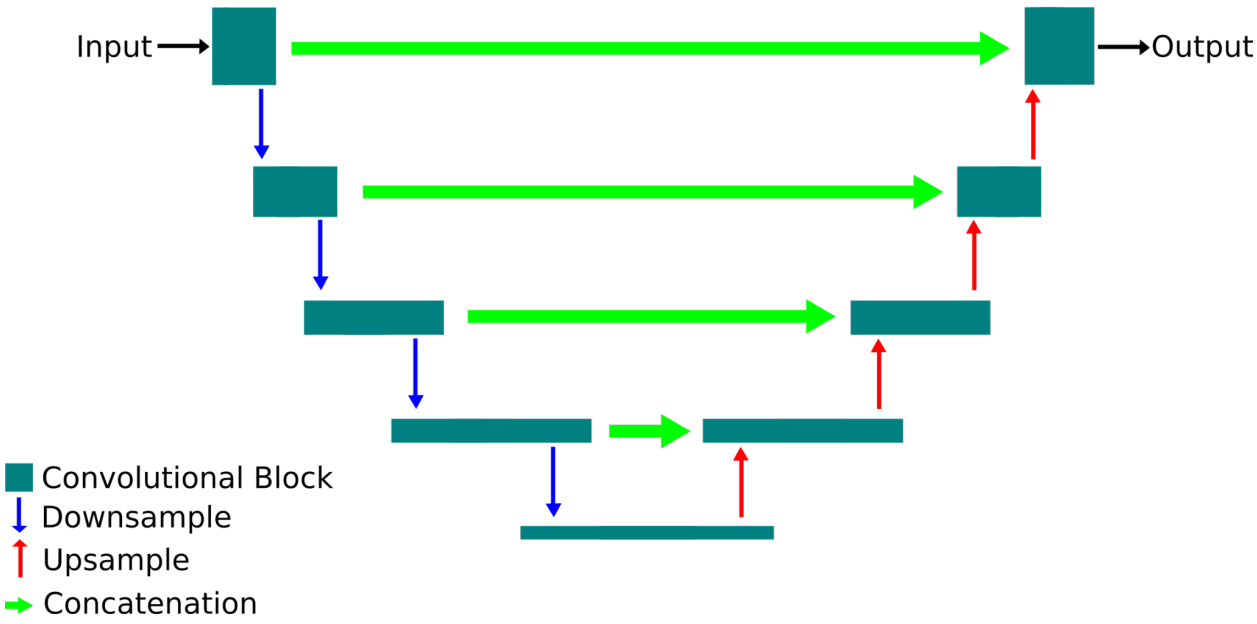

Figure 5: *U-Net model diagram. Dark green polygons represent convolutional blocks, blue arrows represent downsample operations, red arrows represent upsample operations, and green arrows represent concatenation operations.*

Model training and verification were done using regional weather station and ERA5 based daily soil FT observations from the years 2017, 2018, and 2019; whereas, model validation was done against independent observations from years 2016 and 2020. After each epoch the model was verified against observational data from a selection of model training years, and the model with the highest performance score was saved as the final model.

Both Binary Cross Entropy (BCE) and local-variational cost functions (Ruby et al. 2020) were used to maximize the performance of the model FT predictions against the observational FT reference data used for model training. BCE is a standard for binary classification problems such as FT predictions. It takes the model's predicted probabilities for thawed (or frozen) conditions, compares them to the FT reference defined from the observation training data, and then penalizes the neural network based on the distance between the model predicted and expected values. This procedure pushes the model predictions to be closer to 0 (Frozen) or 1 (Thawed) when there is greater confidence in the prediction and closer to 0.5 when the FT status is uncertain. Therefore, in addition to the discrete binary (0 or 1) FT classification, the resulting model provides a continuous variable estimate, ranging between 0 and 1, of the probability of frozen or thawed conditions. Scoring was done using the Matthews Correlation Coefficient (MCC). MCC accounts for true and false positives and negatives when evaluating the model outputs and works even if there is a large class imbalance. The MCC can be calculated using the formula:

$$MCC = \frac{TP\ x\ TN - FPxFN}{\sqrt{(TP+FP)(TP+FN)(TN+FP)(TN+FN)}}, \quad (2)$$

where TP is the number of true positives, TN is the number of true negatives, FP is the number of false positives, and FN is the number of false negatives.

6 - Data Format

The data are provided in individual multi-layer GeoTIFF files for each daily granule in the product time series; where each daily file includes both probabilistic (band 1) and binary (band 2) FT granules. To reduce file size, the product data values are stored as shorts that must be divided by 10,000 to convert back to the original floating point data. This provides a roughly 50% reduction in file size when stored using this method. Once converted back to the original floating point data the data values are defined as follows (Table 1). Separate data files are included for morning (AM) and afternoon (PM) conditions as defined by the satellite overpasses and depicted in the file names.

Table 1. FT variable definitions.

Classification	value
Frozen (binary)	0
Thawed (binary)	1
Thawed probability (low [0] to high [1])	Range: 0-1
Water dominated pixel	-1
Ice dominated pixel	-2
Missing data	-3

Each daily file is projected in the same Northern-Hemisphere Polar EASE-Grid 2 projection format with 9km resolution gridding and 2000x2000 pixels over the domain. The geographical range of the product encompasses Northern Hemisphere land areas (excluding open water and permanent ice dominant grid cells) within -180° to 180° longitude and 0° to 90° latitude.

7 - Data Organization

The data are stored in a hierarchical file structure by year of record from 2016 through 2020. Each daily file is saved using the naming format: *NH_PROBABILISTIC_[AM or PM]_FT_[year]_day[3 digit day of year].tif and ranging* from January first (DOY 001) to

December 31st (DOY 365). The uncompressed individual file sizes are 15.27 MB, while the total multi-year data record is 55.89GB. The entire archive is also available as a compressed zip file (~2.46GB) for more efficient download and storage.

8 - References

Bateni, S.M., C. Huang, S.A. Margulis, E. Podest, and K. McDonald, 2013. Feasibility of characterizing snowpack and the freeze-thaw state of underlying soil using multifrequency active/passive microwave data. *IEEE Transactions on Geoscience and Remote Sensing* 51, 7, 4085-4102.

Brodzik, M.J., B. Billingsley, T. Haran, B. Raup, and M.H. Savoie, 2014. Correction: Brodzik, M.J., et al. EASE-Grid 2.0: Incremental but significant improvements for earth-gridded data sets. *ISPRS Int. J. Geo-Inf.* 3, 3, 1154-1156.

Brodzik, M. J., D. G. Long, and M. A. Hardman, 2021. SMAP Radiometer Twice-Daily rSIR-Enhanced EASE-Grid 2.0 Brightness Temperatures, Version 2 [Data Set]. Boulder, Colorado USA. NASA National Snow and Ice Data Center Distributed Active Archive Center. https://doi.org/10.5067/YAMX52BXFL10.

Danielson, J.J., and D.B. Gesch, 2011. *Global Multi-Resolution Terrain Elevation Data 2010 (GMTED2010)*. US Department of the Interior, US Geological Survey Washington, DC, USA.

Derksen, C., X. Xu, R.S. Dunbar, A. Colliander, Y. Kim, J.S. Kimball, T.A. Black, E. Euskirchen, A. Langlois, M.M. Loranty, P. Marsh, K. Rautiainen, A. Roy, A. Royer, and J. Stephens, 2017. Retrieving landscape freeze/thaw state from Soil Moisture Active Passive (SMAP) radar and radiometer measurements. *Remote Sensing of Environment* 194, 48-62.

Donahue, K., J.S. Kimball, J. Du, F. Bunt, A. Colliander, M. Moghaddam, J.V. Johnson, Y. Kim, and M.A. Rawlins, 2023. Deep learning estimation of northern hemisphere soil freeze-thaw dynamics using satellite multi-frequency microwave brightness temperature observations. *Front. Big Data*, 6, 1243559, doi:10.3389/fdata.2023.1243559.

Dorigo, W., I. Himmelbauer, D. Aberer, L. Schremmer, I. Petrakovic, L. Zappa, W. Preimesberger, et al., 2021. The International Soil Moisture Network: Serving Earth System Science for over a Decade. *Hydrology and Earth System Sciences* 25, 11, 5749–5804.

Du, J., J.S. Kimball, L.A. Jones, Y. Kim, J. Glassy, and J.D. Watts, 2017. A global satellite environmental data record derived from AMSR-E and AMSR2 microwave earth observations. *Earth System Science Data* 9, 2, 791-808.

Entekhabi, D., E.G. Njoku, P.E. O'Neill, et al., 2010. The Soil Moisture Active Passive (SMAP) mission. *Proceedings of the IEEE*, 98, 5, 704-716, doi:10.1109/JPROC.2010.2043918.

Farhadi, L., R.H. Reichle, G.J.M. De Lannoy, and J.S. Kimball, 2015. Assimilation of freeze-thaw observations into the NASA Catchment Land Surface Model. *Journal of*

Hydrometeorology 16, 2, 730-743.

Friedl, M.A., D. Sulla-Menashe, B. Tan, A. Schneider, N. Ramankutty, A. Sibley, and X. Huang, 2010. MODIS Collection 5 global land cover: Algorithm refinements and characterization of new datasets. *Remote Sensing of Environment* 114, 1, 168-182.

Hersbach, H., B. Bell, P. Berrisford, S. Hirahara, A. Horányi, J. Muñoz-Sabater, J. Nicolas, et al., 2020. The ERA5 Global Reanalysis. *Quarterly Journal of the Royal Meteorological Society* 146, 730, 1999–2049.

Kim, Y., J. Kimball, J. Glassy, and K. McDonald, 2021. MEaSUREs Northern Hemisphere Polar EASE-Grid 2.0 Daily 6 Km Land Freeze/thaw Status from AMSR-E and AMSR2, Version 2. NASA National Snow and Ice Data Center DAAC. https://doi.org/10.5067/BDY2V548E07C.

Kim, Y., J.S. Kimball, J. Glassy, and J. Du, 2017. An extended global earth system data record on daily landscape freeze-thaw status determined from satellite passive microwave remote sensing. *Earth System Science Data* 9, 1, 133-147.

Kim, Y., J.S. Kimball, X. Xu, R.S. Dunbar, A. Colliander, and C. Derksen, 2019. Global assessment of the SMAP freeze/thaw data record and regional applications for detecting spring onset and frost events. *Remote Sensing* 11, 11, 1317; https://doi.org/10.3390/rs11111317.

Long, D. G., M. J. Brodzik, and M. Hardman M, 2023. Evaluating the effective resolution of enhanced resolution SMAP brightness temperature image products. *Front. Remote Sens*. 4, 1073765, doi:10.3389/frsen.2023.1073765.

Maeda, T, Y. Yaniguchi, and K. Imaoka, 2016. GCOM-W1 AMSR2 Level 1R Product: Dataset of brightness temperature modified using the antenna pattern matching technique, IEEE TGRS 54, 2, 770-782.

McDonald, K. C., and J. S. Kimball., 2006. Estimation of Surface Freeze-Thaw States Using Microwave Sensors. In *Encyclopedia of Hydrological Sciences*., 53, 1-15, Chichester, UK: John Wiley & Sons, Ltd. https://doi.org/10.1002/0470848944.hsa059a.

McGlinchy, J., B. Johnson, B. Muller, M. Joseph, and J. Diaz, 2019. Application of UNet Fully Convolutional Neural Network to Impervious Surface Segmentation in Urban Environment from High Resolution Satellite Imagery. *IGARSS 2019 - 2019 IEEE International Geoscience and Remote Sensing Symposium*, 3915–18.

Parazoo, N.C., A. Arneth, T.A.M. Pugh, B. Smith, N. Steiner, K. Luus, R. Commane, J. Benmergui, E. Stofferahn, J. Liu, C. Rödenbeck, R. Kawa, E. Euskirchen, D. Zona, K. Arndt, W. Oechel, and C. Miller, 2018. Spring photosynthetic onset and net CO2 uptake in Alaska triggered by landscape thawing. *Global Change Biology* 24, 8, 3416-3435.

Ronneberger, Olaf, Philipp Fischer, and Thomas Brox, 2015. “U-Net: Convolutional Networks for Biomedical Image Segmentation.” In *Medical Image Computing and Computer-Assisted Intervention – MICCAI 2015*, 234–41. Springer International Publishing.

Ruby, A.U., Theerthagiri, P., I.J. Jacob, Y. Vamsidhar, 2020. Binary cross entropy with deep learning technique for image classification. International Journal of Advanced *Trends in Computer Science and Engineering*, 9, 4, https://doi.org/10.30534/ijatcse/2020/175942020.

USDA Natural Resources Conservation Service, 2017. National Water and Climate Center Interactive Map. *USDA National Water and Climate Center*. https://data.nal.usda.gov/dataset/national-water-and-climate-center-interactive-map.

Xu, X., R. S. Dunbar, C. Derksen, A. Colliander, Y. Kim, and J. S. Kimball., 2020. SMAP Enhanced L3 Radiometer Global and Northern Hemisphere Daily 9 km EASE-Grid Freeze/Thaw State, Version 3 [Data Set]. Boulder, Colorado USA. NASA National Snow and Ice Data Center Distributed Active Archive Center. https://doi.org/10.5067/ZV08T8J395JB.

Zwieback, S., A. Bartsch, T. Melzer, and W. Wagner, 2012. Probabilistic fusion of Ku- and C-band scatterometer data for determining the freeze/thaw state. *IEEE Transactions on Geoscience and Remote Sensing 50, 7, 2583-2594.*